

CFD MODELLING OF A NOVEL GRAVITY SEPARATION DEVICE

Christopher B. SOLNORDAL¹, Tim HUGHES², Sandy GRAY², and M. Philip SCHWARZ¹

¹ CSIRO Minerals, Clayton, Victoria 3169, AUSTRALIA

² Gekko Systems, Ballarat, Victoria 3350, AUSTRALIA

ABSTRACT

The InLine Pressure Jig (IPJ) is a novel gravity separation device incorporating a circular bed of solid material that is oscillated to enable the settling of heavier material. The design allows a wide range of operating conditions to be employed, each specifically targeted to maximise the gravity separation of components in a given feed material. CFD modelling of the IPJ was performed to better understand the fluid dynamics taking place within the jig. A transient simulation investigating the flow of a water based slurry containing gold was undertaken. The bed of solids was modelled as an oscillating porous region whose pressure drop behaved in a way similar to a bubbling fluidised bed. The results showed a recirculatory flow pattern within the jig, and enabled an explanation of many of the observed phenomena within the equipment, including bed shape and short circuiting. The model could also be used to investigate the effects of parameters such as bed pulse rate and wave pattern, feed rate, feed properties and ragging makeup, and has proved to be a useful tool in the understanding and design of the InLine Pressure Jig.

TABLE OF SYMBOLS

A	cross-sectional area of the bed (m ²)
D _h	inlet hydraulic diameter (m)
d _p	particle diameter (m)
dp	pressure drop across the bed (Pa)
e _{mf}	bed voidage at minimum fluidising cond'ns (-)
g	acceleration due to gravity (m/s ²)
k _{in}	turbulent kinetic energy at inlet (m ² /s ²)
p	pressure (Pa)
Re _{p, mf}	Reynolds Number of a particle at the minimum fluidising velocity (-)
S _b	momentum source due to bed resistance (N/m ³)
t	time (s)
u	velocity vector (m/s)
u'u'	Reynolds stress tensor (m ² /s ²)
U _{mf}	Minimum fluidising velocity (m/s)
V	average inlet velocity (m/s)
W	weight force of the bed (N)
ε _{in}	turbulence energy dissipation rate at inlet (m ² /s ³)
φ _s	particle sphericity (-)
μ	fluid viscosity (kg/m/s)
ρ	fluid density (kg/m ³)
ρ _s	density of solid feed particles (kg/m ³)

INTRODUCTION

The InLine Pressure Jig (IPJ) is a novel gravity separation device developed by Gekko Systems Pty Ltd (Figure 1). The IPJ incorporates a circular oscillating bed that is fully

encapsulated and pressurised. Water/feed slurry enters the jig via a central feed pipe, and is then distributed radially into a deceleration chamber via a distributor. The solids fall onto a pulsating wedgewire screen where heavier material falls through layers of ragging and is collected in a concentrate stream. Lighter gangue is carried over the tailboard and exits the rig via the tails drainage. The elimination of water free surface improves dynamics within the separation layer and provides significant cost savings in the handling of slurries (Gray, 1997).

The design allows a wide range of operating conditions to be employed, each specifically targeted to maximise separation for a give feed material. The IPJ is currently being operated worldwide to recover free gold, sulphides, native copper, native silver, tin/tantalum, diamonds and garnet. Installations are also planned for coal, lead remediation, magnetite, mineral sands, and iron ore recovery (Gekko Systems, 2006).

Currently, selection of operating conditions (pulsation frequency, amplitude, choice of ragging) is performed based on experience of Gekko Systems' engineers and researchers. However, as it is not possible to observe conditions within the IPJ directly, detailed understanding of the dynamics within the jig is limited. In order to improve this understanding a single phase model of the IPJ-2400 was developed. This paper presents the model methodology and the results of runs using a gold bearing slurry at different feed rates.

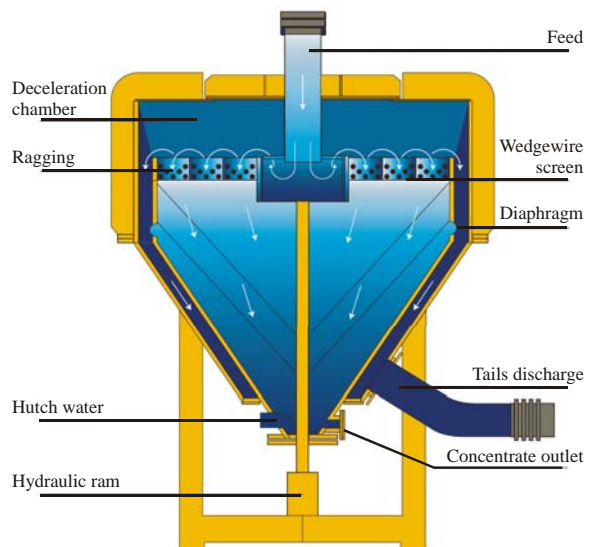


Figure 1: The IPJ-1500, Gekko Systems (2006).

MATHEMATICAL MODEL FORMULATION

The model was formulated using the commercial computational package CFX4.4. The package solves the Reynolds averaged Navier-Stokes equations, treating the slurry as a single phase. The pulsation of the IPJ screen and thick bed is modelled using a moving grid technique, and the solution is therefore transient in nature.

Conservation Equations

To calculate the flow field, the model solves the time-dependent Reynolds averaged Navier-Stokes equations (1) and (2) (AEA Technology, 2001).

$$\frac{\partial \rho}{\partial t} + \nabla \cdot (\rho \mathbf{u}) = 0 \quad (1)$$

$$\frac{\partial}{\partial t} \rho \mathbf{u} + \nabla \cdot (\rho \mathbf{u} \mathbf{u}) = -\nabla p + \nabla \cdot \mu \nabla \mathbf{u} - \nabla \cdot (\overline{\rho \mathbf{u}' \mathbf{u}'}) + S_b \quad (2)$$

The presence of Reynolds stress terms on the right hand side of equation (2), mean that the above equations are not closed. To obtain values for the Reynolds stress terms and close the equation set the standard k- ϵ turbulence model was used (Launder and Spalding, 1974).

Numerical Scheme

Solution of the preceding equations by analytical techniques is not possible. To solve the equations and obtain the flow field, the commercial CFD code, CFX4.4 (AEA Technology, 2001) was used. CFX solves equations (1)-(2) using the finite volume method on a co-located body fitted grid. To avoid checker-board oscillations in the pressure field, the Rhie and Chow (1983) interpolation procedure is used. Coupling between pressure and velocity is achieved using the SIMPLEC algorithm, which is a modified form of the SIMPLE algorithm and is described elsewhere (AEA Technology, 2001; Patankar, 1983). Further details of the solution procedure are given by AEA Technology (2001).

Geometry and Mesh

A dimensioned scale drawing of the two-dimensional axisymmetric geometry of the IPJ-2400 is shown in Figure 2. A slurry containing solid feed and water is passed through the feed pipe under pressure, and enters the distributor. From here the slurry is directed into the deceleration chamber, where solids settle out onto the screens to form a thick bed of solid particulate material. Heavy material passes through the ragging and screens into the hutch and out through the concentrate outlet. Settling of lighter material is hindered by the pulsation of the screens and thick bed, and this material passes between the inner and outer cones to the tailings outlet. Other than the location of the tailings outlet, the IPJ is axisymmetric about the feed pipe centreline, and is therefore modelled using a two-dimensional axisymmetric mesh to minimise computational effort. The hexahedral mesh has approximately 12,400 cells and a detail of it is shown in Figure 3. Ragging and bed material is modelled as a porous region of flow.

Separate routines were employed to recalculate the position of the grid at each time step through the screen pulsation cycle. Terms specifying the local grid velocity

were added to Equations (1) and (2), and the transient terms were also modified to allow for the possibility of changing volume of each cell with time.

The profile of the thick bed of feed material was estimated by operators to be as shown in Figure 3 (based on plant observations after removal of the IPJ lid), and remained constant throughout the simulation.

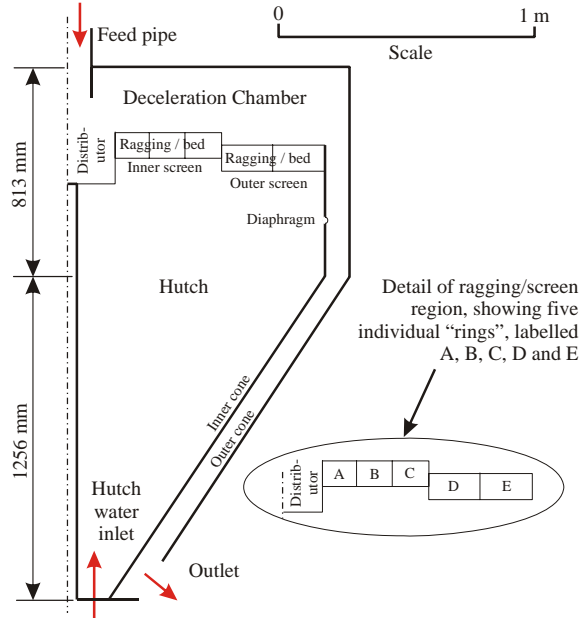


Figure 2: Elevation view (to scale) of IPJ 2400, showing significant dimensions and screen ring detail.

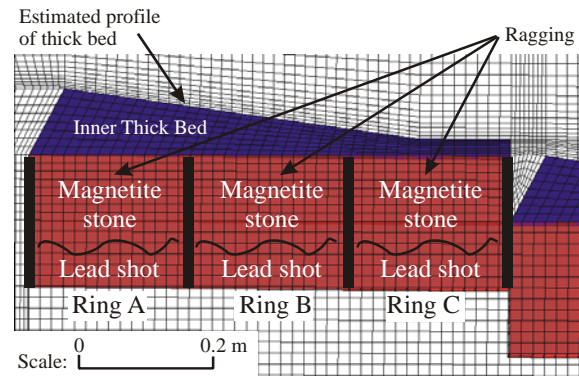


Figure 3: Mesh detail around the inner ragging and thick bed. The three inner rings (A, B and C) are shown.

Boundary Conditions

The feed pipe and hutch water inlets were modelled as Dirichlet boundaries. Turbulence quantities were estimated at the inlets using empirical functions (Equations (3)) suitable for use with small inlets entering a large flow domain (AEA Technology, 2001).

$$k_{in} = 0.002 V^2; \quad \epsilon_{in} = k_{in}^{1.5} / (0.3 D_h) \quad (3)$$

All solid surfaces were modelled as no-slip wall boundaries with wall functions. The tailings exit was modelled as a constant pressure boundary.

The screens, ragging and thick beds were modelled as porous regions. Through these regions the voidage (and

hence the flow area) was specified, and velocities increased as a function of this area. Also, the pressure drop through the porous region was specified using a body force, S_b (see Eq. (2)), which was proportional to the local velocity slurry.

To determine the porous region pressure drop, dp , the ragging and bed was assumed to act like a bubbling fluidized bed which has a standard pressure vs. velocity curve (Figure 4). With this distribution the pressure drop through the bed increases linearly with bulk velocity through the bed up to the point where the pressure drop is equal to the weight of the bed, W , divided by the bed's cross-sectional area, A . This transition occurs at the minimum fluidizing velocity, U_{mf} . Beyond this point the pressure across the bed remains constant while the particles in the bed move apart and increase the flow area.

U_{mf} for a given ragging material was determined using the correlation Equation (4) (Kunii and Levenspiel (1991) as a function of bed voidage at minimum fluidising velocity, e_{mf} , and particle sphericity, ϕ_s .

$$\frac{1.75}{e_{mf}^3 \phi_s} \text{Re}_{p,mf}^2 + \frac{150(1-e_{mf})}{e_{mf}^3 \phi_s^2} \text{Re}_{p,mf} = \frac{d_p^3 \rho(\rho_s - \rho)g}{\mu^2} \quad (4)$$

Typical graphs of U_{mf} vs voidage are shown in Figure 5 for magnetite stone ragging and thick bed feed material. From this data the velocity through the bed, and hence the pressure drop across the bed, could be determined at any given time in the pulsation cycle. U_{mf} for the stones was greater than 0.15 m/s, which is equal to the down stroke velocity of the screens, and the value for lead shot was greater still. For gold feed material, U_{mf} was approximately equal to 0.015 m/s, a value much less than the down stroke velocity of the screens. Thus it was assumed that the ragging remained packed under all conditions, whilst the feed material expanded to a voidage of approximately 0.6. Kunii and Levenspiel (1991) report that voidage of a randomly packed bed of near-spherical particles is equal to 0.37 ± 0.5 (Kunii and Levenspiel, 1991, page 64, Figure 1), depending on the density of packing and the sphericity of particles. For this work it was assumed that the ragging packed to a voidage of 0.45.

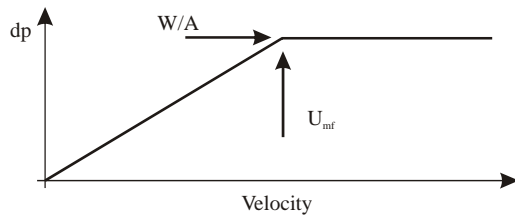


Figure 4: Fluidisation characteristic curve, showing transition to fluidisation at U_{mf} .

RESULTS

A total of three runs were performed in this investigation, and their conditions are summarized in Table 1. Run 1 was a base case using typical conditions for processing gold-bearing feed. The two additional runs investigated changes in feed rate (Runs 2 and 3). Runs were modelled under pulsing conditions for a total of three saw-tooth pulse cycles (Figure 6).

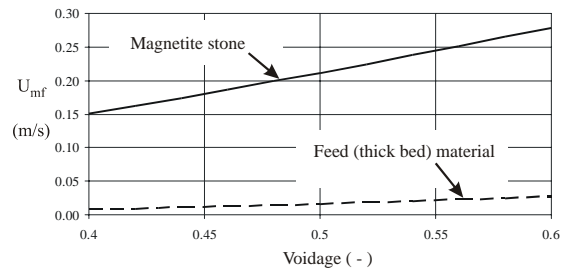


Figure 5: U_{mf} for magnetite stone and feed (using Eq. (4)).

Slurry / hutch water properties				
Property	Run 1	Run 2	Run 3	
Slurry feed rate (tph)	160	80	40	
Hutch water feed rate (L/min)	8	4	2	
Slurry Density (kg/m ³)	1300 (50/50 wt% feed/water)			
Slurry Viscosity (kg/m/s)	0.001			
Ragging / thick bed properties				
Layer	Material	Diameter (mm)	Thickness (mm)	Voidage (-)
Ragging layer 1	Lead shot (s.g. = 11)	8.4	8.4	0.45
Ragging layer 2	Magnetite stone (s.g. = 5)	18	90	0.45
Thick bed	Feed material (s.g. = 3)	1	See Fig. 9	0.6

Table 1: Summary of run conditions.

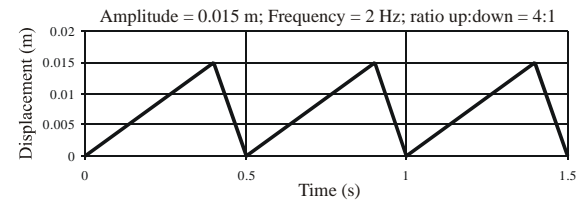


Figure 6: Details of saw-tooth pulsation waveform.

Run 1: 160 tph feed rate

The overall flow field predicted for Run 1 is shown in Figure 7 at the top of the suction stroke ($t = 0.90$ s). The flow is quantified using velocity vectors (length proportional to speed) as well as contours coloured relative to the magnitude of the vertical velocity. Thus dark blue areas represent down-flow and red areas represent up-flow.

The white arrows in Figure 7 show the overall flow pattern. Feed enters vertically through the feed pipe, and is re-directed into the deceleration chamber via the distributor. Some slurry is predicted to recirculate in the deceleration chamber (shown in more detail in Figure 8), while the remainder passes between the inner and outer cones to the tailings exit. Flow in the hutch shows a large recirculation, however, this flow did not affect flow through the screens or in the bed or deceleration chamber. During the downstroke, the overall flow pattern remained the same as for the suction stroke, except that a large amount of hutch water was forced through the screens and bed, as expected.

Detailed velocity vector plots for flow through the bed and deceleration chamber are shown in Figure 8 for a series of three time steps (shown as pink squares in Figure 8). At $t = 0.9$ s (Figure 8 (a)) the screens are at the top of the suction stroke. After entering through the feed pipe and distributor, the flow slows down in the deceleration chamber near the roof. There is a clear recirculation in the deceleration chamber (red arrow). Hutch water passes up through both the inner and outer screens. For Rings B, C, D and E the upward velocity is only 1-2 mm/s. At Ring A the velocity is higher, and reaches a maximum of greater than 60 mm/s at the ring's inner edge. This is because the upward velocity from the entry stream is approximately 1.25 m/s within the circle labelled L in Figure 8 (a), which causes a low pressure region at the inner edge of the ring.

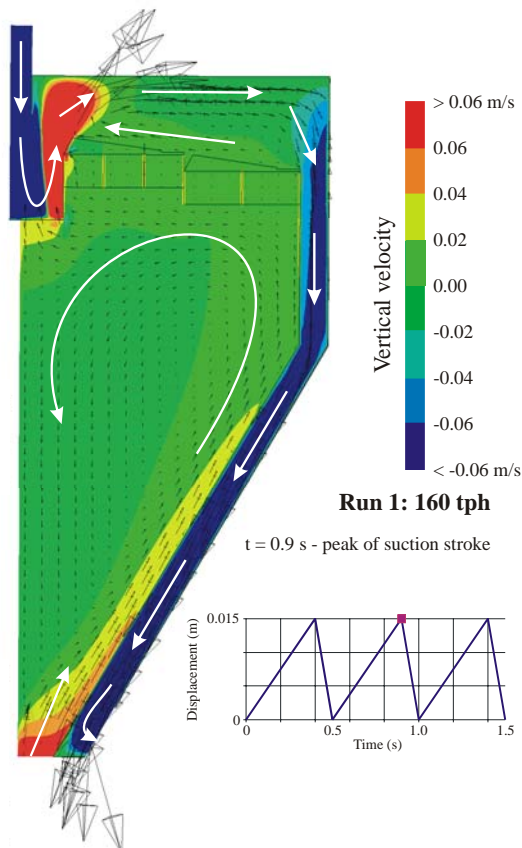


Figure 7: Velocity (black vectors) and the vertical velocity component (coloured contours) at time $t = 0.90$ s for Run 1.

At $t = 0.92$ s (Figure 8 (b)) the screens have just commenced their downstroke, and the velocities through the screens and bed are increased. The upward velocity through Ring A is now at least 20 mm/s, and the region of flow that is greater than 60 mm/s extends across about 1/3 of the ring. Velocity in Ring B is uniform and greater than 20 mm/s, and for Ring C is approximately 10 mm/s. The fluid in outer Rings D and E has a uniform upwards velocity of about 6 mm/s. In this case velocities are higher at the inner rings due to the hutch water that is displaced from beneath the feed distributor (white arrow in Figure 8 (b)).

Figure 8 (b) also shows that the upflow in the deceleration chamber above the thick bed is significantly increased. Velocity vectors above the thick beds at $t = 0.90$ s were

approximately horizontal, whereas at $t = 0.92$ s they are up to 45° from horizontal. This upflow lifts particles in the thick bed, allowing it to partially fluidise. The cross flow component causes material to be carried back towards the centre of the deceleration chamber, and produces the wedge-shaped thick beds that are observed in practise.

At time $t = 1.04$ s (Figure 8 (c)) the screen has commenced the suction stroke. Velocities throughout all rings are only about 1 mm/s, and the flow in the deceleration chamber above the thick beds is once more close to horizontal. The flow at the inner edge of Ring A has developed a recirculation, which probably limits the angle at which the thick bed makes with the inner edge of the inner ring. By $t = 1.08$ s the up flow at the inner edge of Ring A is re-established, and by time $t = 1.40$ s (top of the suction stroke) the flow is similar to that at $t = 0.9$ s (Figure 8 (a)).

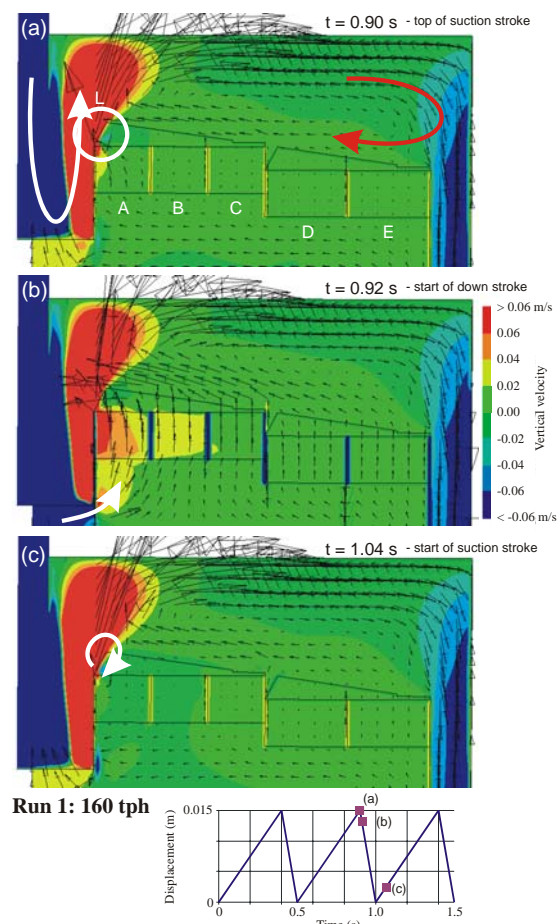


Figure 8: Velocity (black vectors) and vertical velocity components (coloured contours) at (a) $t = 0.90$ s; (b) $t = 0.92$ s; (c) $t = 1.04$ s, for Run 1.

A second set of vector plots is shown in detail for the flows through Rings A and B in Figure 9. At $t = 0.9$ s (top of the suction stroke, Figure 9 (a)). Recirculating flow travels toward the centreline along the surface of the thick bed. As the downstroke commences (Figure 9 (b)) there is strong up-flow through both Rings A and B causing the bed to fluidise. This behaviour continues throughout the downstroke (Figure 9 (c)). As the suction stroke commences (Figure 9 (d)) the flows through the rings are

close to zero, and two local recirculations are set up. The first is at the edge of the inner ring, while the second is along the surface of the thick bed, causing flow away from the centreline in a thin layer above the bed surface. This second recirculation is short lived, and is no longer evident at $t = 1.08$ s (Figure 9 (e)).

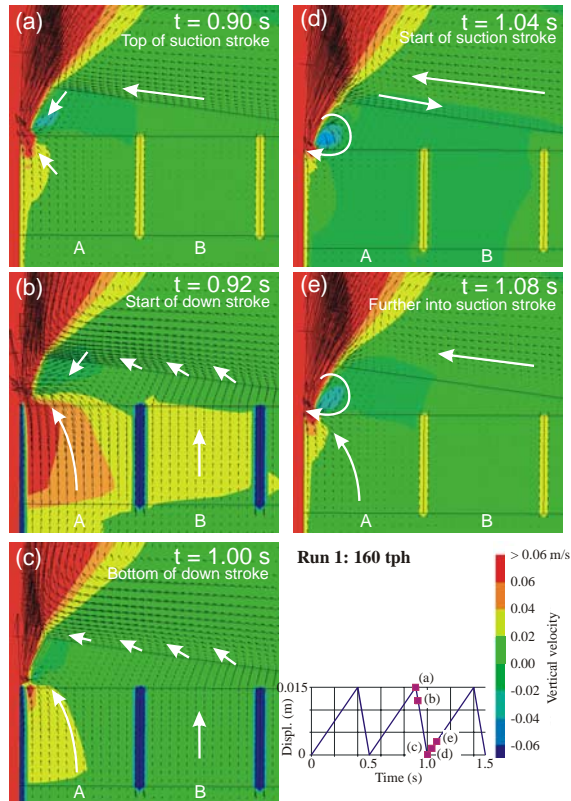


Figure 9: Velocity (black vectors) and vertical velocity components (coloured contours) through Rings A and B at (a) $t = 0.9$ s; (b) $t = 0.92$ s; (c) $t = 1.00$ s; (d) $t = 1.04$ s; (e) $t = 1.08$ s, for Run 1.

Runs 2 and 3: Varying Feed Rate

Runs 2 and 3 use 80 and 40 tph slurry rate, compared to 160 tph for Run 1, with hutch water flow rates reduced in the same proportion. Figure 10 shows the velocity vector field in the deceleration chamber and upper hutch region for Run 3. The strength of the recirculation in the deceleration chamber is predicted to decrease with feed rate, and in Figure 10 (40 tph feed rate, suction stroke) the recirculation has been eliminated. More detail of the flow patterns is provided in Figure 10 (b) for Rings A and B, where it can be seen that the flow travels along the top of the thick bed towards the outer cone, in contrast to Run 1.

Particle Tracks

In order to gain an understanding of where different sized feed particles might congregate in the IPJ, Lagrangian particle tracking was employed as a post-processing step. Figure 11 shows the distribution of particle tracks of different sizes and densities as they pass from the IPJ for Runs 1 and 3. Although the particles are tracked through the thick beds and ragging, their accuracy is poor in these regions.

In Run 1, using particles of 3000 kg/m^3 (Figure 11 (a)) most particles are predicted to settle on to the thick beds. The smaller particles are carried towards the outer rings, whilst the larger particles only carry as far as Ring C. This effect is further emphasised when using particles of 8000 kg/m^3 (Figure 11 (b)), with almost all particles shown to travel only as far as Rings A and B.

For Run 3 using a feed rate of only 40 tph, the particles are predicted to settle on Rings A and B only, suggesting that at this feed rate the thick bed profile would be considerably different to that assumed in Figure 3.

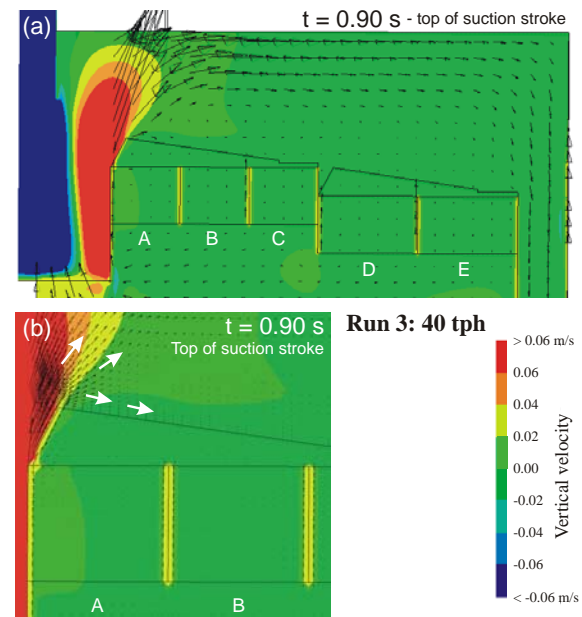


Figure 10: Velocity (vectors) and vertical velocity components (coloured contours) at $t = 0.9$ s (a) all rings; (b) Ring A and B detail. Run 3.

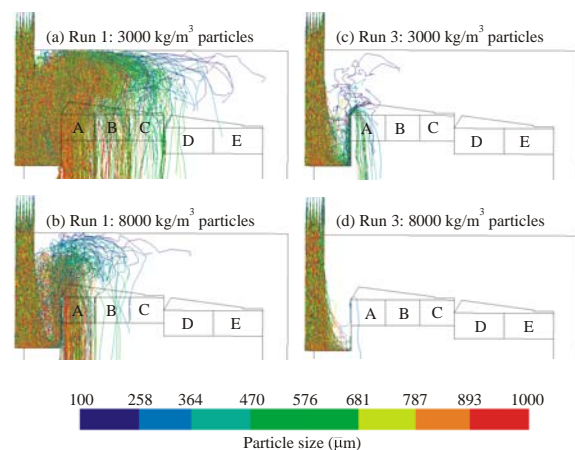


Figure 11: Variation in particle track location with particle density and size – Run 1 and Run 3.

DISCUSSION

Flow in the Deceleration Chamber

Gekko's design of the IPJ was previously thought to generate a plug flow in the deceleration chamber (Gray, 1997), where slurry travelled horizontally from the centre to the outside of the chamber with larger/heavier solids falling quickly to the surface of the thick bed and

lighter/smaller solids being carried more towards the outer edge. The modelling work has consistently shown that instead, a recirculating flow exists that is predicted to carry material over the surface of the thick bed towards the centreline of the jig. Thus the model suggests the bed is thicker centrally not only because large solids drop out quickly, but also because smaller material is carried back towards the centreline of the jig by the recirculation.

The velocity of slurry across the top of the deceleration chamber is necessarily higher due to the recirculation, and this aids in the distribution of solid material across the full radius of the bed. Of the material carried to the outer radius of the jig, a proportion is caught in the recirculation and carried back over the thick bed, thus increasing its residence time in the deceleration chamber. The model shows that material on the thick bed is thrown up into the deceleration chamber by the jiggling motion of the screens, and gradually moved back towards the jig centreline. Consequently, it is thought that the overall effect of the recirculation is beneficial to the jig operation.

The tracking of particles through the deceleration chamber indicates that heavy solids fall onto the inner rings despite the recirculation. However the small, light particles are shown to be carried back towards the centreline of the jig before falling onto the thick bed.

It was found that the recirculation can be prevented by using a very low feed rate (40 tph, Run 3). However, even then it is only stopped during the suction stroke, and reappears during the down stroke of the screens.

Dynamics of the Thick Bed

The thick bed was modelled as a porous solid whose shape and thickness did not change during the pulsation cycle. The voidage of the bed was specified to be 0.6, compared to the ragging which has a voidage of 0.45. Thus the thick bed was assumed to always be partially fluidised. In reality the thick bed is likely to be constantly expanding and contracting with the screen pulsation. Model results show high vertical velocity of slurry through and above the thick bed during the down stroke of the screens, greater than the fluidisation velocity of the feed material. This is an aspect of the current model that could be improved by specifying a variable porosity of the thick bed, as well as a variable thickness of the bed. By modelling the slurry as a two-phase mixture of solids and water it would be possible to predict the profile of the thick bed and how it varies during the pulsation cycle.

Flow Through the Screens and Ragging

The modelling indicated that hutch water short-circuiting occurs at the inner edge of Ring A primarily because of the high velocity of slurry exiting the distributor causing a low pressure region there. Plant observations support this finding, with little or no build up of material at this location. Also, a small eddy is predicted to occur (see Figure 9 (d) and (e)), further limiting the build up of solids there and providing the thick bed with its characteristic profile at the inner ring.

In general the velocity through the rings decreases from Ring A (inner) to Ring E (outer). During the suction stroke the velocities through Rings B-E are very low for

the conditions studied, and care must be taken to ensure hutch water flow rates are adequate to prevent back flow through the screens.

Limitations of the Model

The main limitation of the current model is the treatment of the slurry as a single phase. As a consequence, the thick bed profile and voidage must be specified and this does not change during the pulsation cycle. When considering significantly different processing conditions (such as Run 3 compared to Run 1) the assumed distribution of solids on the thick bed is not known and may be in error, and it is not possible to determine what effect this error will have on model performance. Furthermore, very little information regarding the effect of ragging choice on jig performance (sharpness of cut) can be determined.

It is recommended that future modelling involve two approaches: (1) a detailed discrete element modelling simulation of a small portion of the ragging and thick bed, which would provide information on the effect of interactions between particles of different size and density on the relative motion through the bed and ragging, and (2) a two-phase model allowing prediction of the dispersion of solids throughout the system.

CONCLUSIONS

A two-dimensional single-phase model of Gekko Systems' IPJ-2400 in line pressure jig has been developed and used to investigate its performance. It was found that slurry recirculates within the deceleration chamber, spreading solid material more evenly across the screens and increasing residence time of the recirculating solid material within the chamber. Despite the recirculation, heavier solid material is predicted to quickly fall onto the thick bed near the inner rings of the screen. However, short-circuiting is predicted to occur at the same location due to high velocity of the slurry exiting the distributor.

REFERENCES

- AEA TECHNOLOGY, (2001), CFX-4.4: Solver Manual, AEA Technology, Harwell Laboratory, Oxfordshire, UK.
- GEKKO SYSTEMS, (2006), Company internet site at <http://www.gekkos.com.au>
- GRAY, A.H., (1997), "InLine Pressure Jig – An exciting, low cost technology with significant operational benefits in gravity separation of minerals", *The AusIMM Annual Conference*, Ballarat, 12-15 March 1997, 259-265.
- KUNII, D. and LEVENSPIEL, O., (1991), *Fluidization Engineering*, 2nd Edn, Butterworth-Heinemann.
- LAUNDER, D.E. and SPALDING, D.B., (1974), "The Numerical Computation of Turbulent Flows", *Comp. Meths. Appl. Mech. Engng*, **3**, 269-289.
- PATANKER, S.V., (1983), *Numerical Heat Transfer and Fluid Flow*, Hemisphere.
- RHIE, C.M. and CHOW, W.L., (1983), "Numerical study of the turbulent flow past an airfoil with trailing edge separation, *AIAA J*, **21**, 1527-1532.